Master thesis

Scanning Superconducting Quantum Interference Device Microscopy

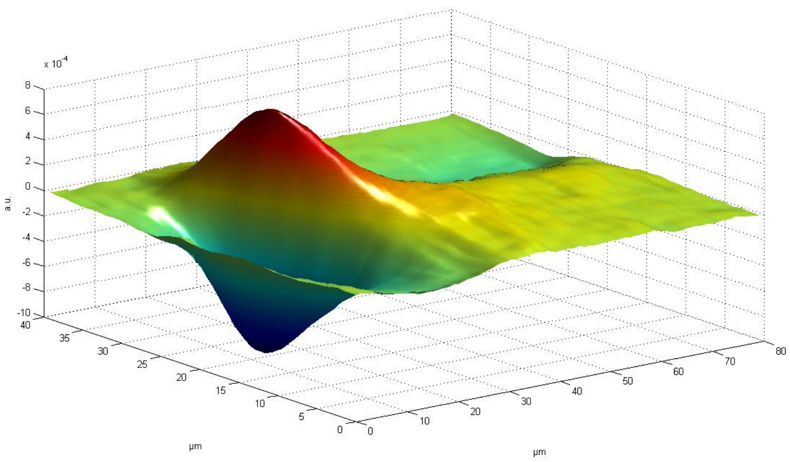

Sensitive mapping of magntic flux on thin films

Tom Wijnands

January 2013

Scanning Superconducting Quantum Interference Device Microscopy

By

Tom Wijnands

To obtain the degree of Master of Science,
Applied Physics

January 10^{th}, 2013

Abstract

Thin films and interfaces can hold interesting phenomena. A scanning superconducting quantum interference device microscope (SSM) can map the magnetic flux of a surface. With a SSM a high magnetic resolution can be achieved. The SSM at the University of Twente has been made operational again. Improving the fabrication processes and making the setup more robust. Three different materials have extensively been tested using this device. The first material is a $LaAlO_3/SrTiO_3$ interface which might have ferromagnetism and superconductivity in a single interface. This was not found in the tested samples. In the second material doped TiO_2 a landscape of ferromagnetic dipoles were found. The third material a $LaMnO_3$ (LMO) film. The LMO films are grown on STO and are ferromagnetic insulators. Measuring the LMO films with the SSM revealed ferromagnetic domains.

Exam committee:
Prof. Dr. Ir. H. Hilgenkamp
Dr. M.H.G. Duits
Dr. Ir. J. Flokstra
P.D. Eerkes MSc
Ing. D. Veldhuis

Work preformed at:
Interfaces and Correlated Electron systems group
Faculty of Science and Technology
University of Twente
P.O. Box 217
7500 AE, Enschede

Contents

Chapter 1

Introduction

For centuries people have studied nature. Searching for the physics behind it and improving technology by doing so. Materials science is a part of that quest. Many discoveries have been made in this field. One of these findings is that thin films can have different properties as the bulk material. There are different scanning techniques for measuring properties of thin films. Examples of these techniques are atomic force microscopy (AFM) and scanning tunneling microscopy (STM) [1, 2]. The discovery of superconductors and the creation of the Josephson equations are at the basis of a new device that can measure small magnetic fields. This device is called a Superconducting Quantum Interference Device (SQUID) and was created in 1964 [3].

A small SQUID can be placed on motion controllers making the SQUID able to move over a surface of a sample. This device called a scanning SQUID microscope (SSM). The first device called a SSM was made in 1993 [4]. This device is a two dimensional SSM. The SSM maps the magnetic flux of a sample surface. A SQUID can only operate at low temperatures, because it consists of superconducting materials. This means that either the sensor and sample are submerged into liquid helium or nitrogen, or the sensor is cooled using a gas flow. The second option has the advantage that the samples can be at different temperatures, including room temperature. This can be interesting for organic samples [5–7].

There are many different measuring techniques for measuring local magnetic field on a sample surface. All techniques have some advantages and disadvantages over each other. Figure 1.1 displays some different techniques comparing their spatial and magnetic resolutions. At one end of the spectrum is the SSM. Scanning SQUID microscopes have a very high magnetic resolution. However the SSMs have a limited spatial resolution. This is due to the size of the pickup loop and SQUID itself. On the other end of the spectrum there is magnetic force microscopy (MFM) [8]. This technique is similar to an AFM. A sharp magnetized tip moves over the sample and measures the tip-sample interactions. These interactions resemble the magnetic properties of the sample. This technique has a very high spatial resolution, but this comes at the cost of the magnetic resolution.

The SSM at the University of Twente is donated by IBM TJ Watson research center in Yorktown Heights, NY, USA. In this setup, sample and sensor are submerged in a large cryostat filled with liquid helium, which is at a temperature of 4.2 K. The SQUID sensor has been modified for SSM purposes. The most noticeable of these modifications are that a pickup loop is attached to the SQUID ring[9–11]. The sensor can now pickup magnetic flux closer to the sample surface. The SSM setup in Twente has not been operational for the last 1.5 years. Maintaining and operating a SSM is a difficult and time consuming operation.

This thesis describes the procedures for making the SSM operational again. The problems that were encountered and the solutions that were found. Some general superconducting theory is given in Chapter two. The focus in this chapter is on the basic principles of a SQUID. In the third chapter the

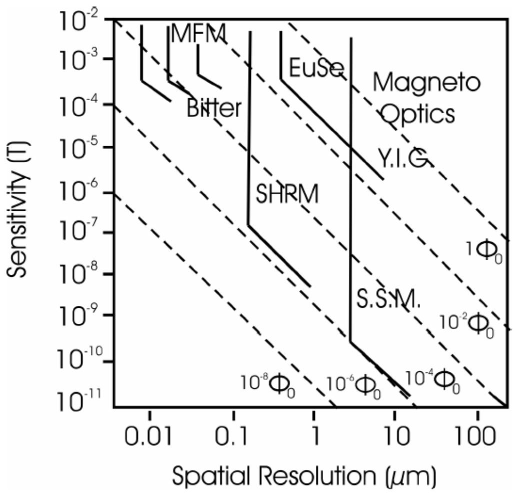

Figure 1.1: The magnetic and spatial resolutions of different magnetic microscopy techniques. This figure was published in [7].

experimental setup is explained. The changes that were made to the SSM to make it more reliable. The procedures to replace and repair the parts of the setup are also highlighted. The research that was done using this microscope is shown in chapter four. Finally in chapter five conclusions are drawn and recommendations are made.

Chapter 2

Theory

2.1 Introduction to superconductivity

Heike Kamerlingh Onnes discovered superconductivity in 1911 in Leiden. Superconductivity is one of many a quantum mechanical effects that occur in nature. In a superconductor electrons flow with zero resistance. Ohms law states that zero resistance means that superconducting materials can conduct a current without any voltage being applied. No energy dissipates during the transport process. Superconducting materials become superconducting when they are below a critical temperature (T_c). This temperature is material dependent and usually very low, in the order of a few Kelvin.

Next to the zero resistance phenomena, superconductors show another important effect. They tend to repulse all magnetic fields from the superconducting material. This effect is called the Meissner effect. Magnetic fields break down the superconductivity, when a high external magnetic field is applied superconducting materials lose their superconducting effects when it is above a critical magnetic field. The breakdown can be classified into two groups. Type one superconductors lose their superconductivity and behave as a normal material, when the external magnetic field is increased above a critical value (Bc), as figure 2.1 (a). In type two superconductors there is a mixed state between complete repulsion and losing the superconducting effects. In this state the magnetic field locally penetrates the superconductor creating so called Abrikosov vortices when the field strength is above Bc1, as figure 2.1 (b). The type two superconductors behave as a normal material when the field strength is above Bc2. Yttrium Barium Copper Oxide (YBCO) is an example of a type two superconductor[12].

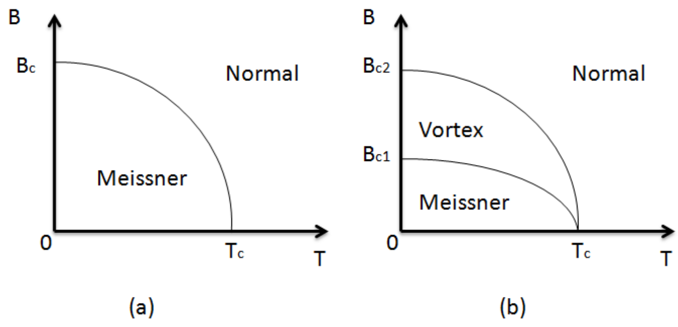

Figure 2.1: The magnetic state of the superconductors depending on temperature and magnetic field. (a) Type one superconductors. When a external magnetic field is above Bc the material behaves as a normal metal. (b) Type two superconductors. When a external magnetic field is between Bc1 and Bc2, the magnetic field penetrates the superconductor locally in the form of vortices. Above Bc2 the material behaves as a normal metal.

These phenomena are strange compared with normal conducting behavior. In a normal metal it is possible to view electrons as a ”fluid” flowing though the atomic lattice. The electrons constantly collide with the atoms in lattice. The collisions transform kinetic energy into heat and therefore the transport of electrons lose kinetic energy. This loss is a cause for electric resistivity.

In a superconductor individual electrons pair up into a Cooper pair named after Leon Cooper. The paired electrons behave as bosons and through electron-phonon interactions they are bound together. Cooper pairs occupy a single ground state and can be described a macroscopic wave function $\psi = |\psi|e^{i\varphi}$. Here φ is the phase of the wave function (ψ). The theory describing superconductivity is called Bardeen-Cooper-Schrieffer (BCS) theory [13]. The superconductor with the highest critical temperature is mercury barium calcium copper oxide with a temperature around 135 K [14].

2.2 Josphson junctions

A Josephson junction is a junction between two superconducting materials with a weak barrier in between. Examples are a Superconductor-Insulator-Superconductor(SIS) junction or a Superconductor-Normal Metal-Superconductor(SNS) junction. According to BCS theory electrons pair up into Cooper pairs. The Cooper pairs in the superconductor tunnel through this barrier. Tunneling causes a phase shift in the wave function of the paired electrons. The equations to describe such a barrier were made by Brain Josephson for which he won the Nobel prize in physics in 1973 [15].

$$I_s = I_c \sin \varphi \tag{2.1}$$

$$V = \frac{\hbar}{2e}\frac{d\varphi}{dt} \tag{2.2}$$

The first Josephson equation (2.1) describes the supercurrent that flows through the junction. This super current (I_s) is dependent on the critical current(I_c) and phase difference(φ) over the weak barrier. The first equation is also called the DC Josephson effect. The second Josephson equation (2.2) describes the voltage over the junction. The voltages changes the phase shift over the weak barrier. It causes the phase shift to oscillate over time. The second equation is also called the AC Josephson effect.

For a Josephson junctions in the voltage state the Resistively and Capacitively Shunted Junction(RCSJ) model is used to simulate the ideal situation. In the model the current flowing through the system is the sum of the three individual currents flowing. The flowing currents are the Josephson current, shunt current and a transport current due to capacitance [16, 17]. This adds up to the following equation:

$$I = C\frac{dV}{dt} + I_c \sin \varphi + \frac{V}{R} \tag{2.3}$$

Due to the complexity of this equation finding an analytical solution can only be done in a limited amount of situations, since the voltage is dependent on the phase change over time. However it can be solved numerically. If there is a voltage over the Josephson junction, there will be an oscillating Josephson current over time. The oscillating current makes solving the second order differential equation (2.3) even harder. Such an oscillation can be countered with a high capacitance in the SQUID circuit. The damping parameter is called the Steward-McCumber parameter (β_c) [18, 19]. The oscillations are damped if the Steward-McCumber is lower than one. The Steward-McCumber is defined as:

$$\beta_c \equiv \frac{2e}{\hbar} R_n^2 I_0 C \tag{2.4}$$

2.3 Flux quantization

BCS theory describes superconductivity. This theory states that the electrons pair up into Cooper pairs and that the current in a superconducting ring is quantized. These Cooper pairs are described with a wave function. The phase of this wave function depends on the current density (J_s) and the vector potential (A), as can be seen in equation (2.5).

$$\Delta\varphi = 2\pi\left(\frac{2m}{hn_s e}J_s + \frac{2e}{h}A\right) \tag{2.5}$$

The single valuedness of the wave requires that the phase difference in a superconducting ring is equal to an integer times 2π. This gives rise to a flux which is quantized.

$$\Delta\varphi = 2\pi\frac{2e}{h}\left(\frac{m}{n_s e^2}\int J_s dl + \int Adl\right) = 2\pi\frac{2e}{h}\phi = n2\pi \tag{2.6}$$

Here the magnetic field is related to a magnetic flux quantum (ϕ_0). A flux quantum is defined as: $\phi_0 = h/2e = 2.07 \cdot 10^{-15} Wb$. This can be simplified further when the integrated area is much larger than the penetration depth, the equation reduces to:

$$\int BdA = \phi = n\phi_0 \tag{2.7}$$

2.4 DC SQUID

The direct current superconducting quantum interference device (DC SQUID) is one of the most sensitive magnetic sensors [20]. It consists of two Josephson junctions parallel to each other placed inside a superconducting ring. As can be seen in picture 2.2(a).

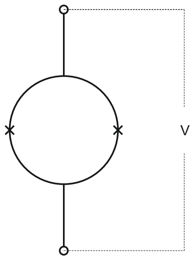

(a)

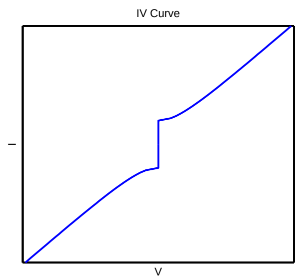

(b)

Figure 2.2: (a) A schematic view of a SQUID. Two Josephson junctions are connected parallel in a superconducting ring. (b) Sketch of IV curve over a Josephson junction.

The combination of flux quantization together with the Josephson effect causes this system to be a sensitive magnetic sensor. The critical current that flows though the system is the sum of the individual junctions, simply following Kirchoff's law.

$$I = I_{c1}\sin\varphi_1 + I_{c2}\sin\varphi_2 \tag{2.8}$$

Combining the current over the two Josephson junctions with the flux quantization equation (2.6) gives a relation between magnetic field and the current (2.9). Here the assumption is made that the width of the superconducting material in the SQUID ring is thicker than the London penetration depth, so $J_s = 0$.

$$I = I_0 \sin \varphi_0 \cos \pi \frac{\phi}{\phi_0} \tag{2.9}$$

2.5 Flux locked loop

A SQUID has a non linear periodic flux to voltage conversion. The most sensitive way to operate a SQUID is using the flux locked loop (FLL) mode [21]. A schematic view of such a setup is show in figure 2.3. The SQUID operates at a constant bias current. A modulated triangular wave is applied. One period of the applied signal corresponds roughly with one ϕ_0. A working point is chosen by setting the DC offset to 0 Volt.

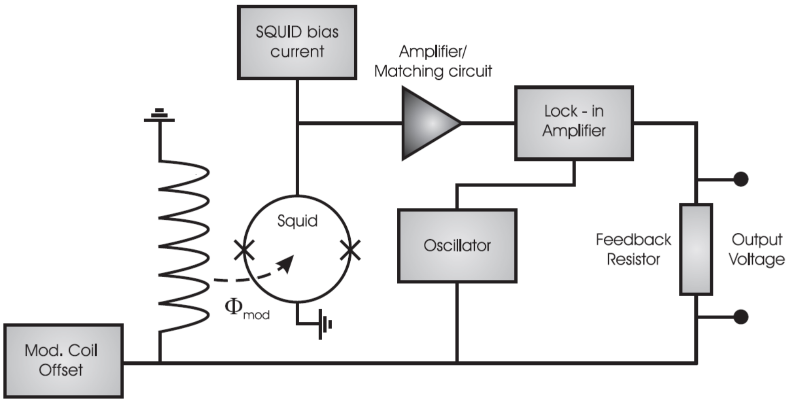

Figure 2.3: Schematic view of a basic FFL setup. This figure was published in [22].

When the signal from the SQUID gets locked by the lock-in amplifier a working point is created. External flux that is picked up by the SQUID gives a DC offset to the working point making it a non zero value. The offset voltage is a direct measure for the external flux. With a flux locked loop operating method very low noise levels can be reached. The typical white background noise level is around a few $\mu\phi_0/\sqrt{Hz}$.

2.6 Dipole Model

One of the common features on the scanning SQUID measurements are magnetic dipoles. To give insight on the source of these ferromagnetic effects a magnetization value should be calculated. A method to do this is to create a model for the magnetic field and fit this to the measured data [23]. The experimental situation is displayed in figure 2.4.

Here the SQUID pickup loop is above the surface of the sample and measures the magnetic field of

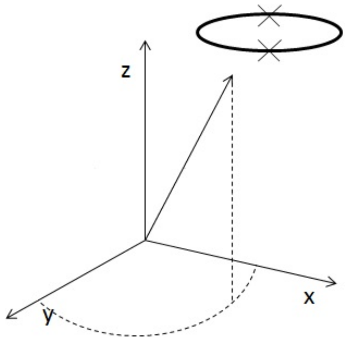

Figure 2.4: A schematic view of a SQUID loop at a distance from a dipole source.

a dipole at a certain distance and height from its center. The pickup loop of the SSM only picks up the out of plane magnetic fields. By fitting a model to the measured data it is possible to calculate the magnetic moment of the dipole. The magnetic field for a dipole can be derived from Biot-Savart equation. The assumption is that the dipoles consist out of two magnetic point sources.

$$B = \frac{\mu_0}{4\pi} \int \frac{Idl \times r}{|r|^2} \tag{2.10}$$

When this is solved in three dimensions and rewritten ($B = B_x + B_y + B_z$) in Cartesian coordinates, the equations become:

$$B_{z,x}\left(x, y, z\right) \frac{\mu_0}{4\pi} 3m_x \frac{xz}{\left(x^2 + y^2 + z^2\right)^{5/2}} \tag{2.11}$$

$$B_{z,y}\left(x, y, z\right) \frac{\mu_0}{4\pi} 3m_y \frac{yz}{\left(x^2 + y^2 + z^2\right)^{5/2}} \tag{2.12}$$

$$B_{z,z}\left(x, y, z\right) \frac{\mu_0}{4\pi} m_z \frac{3z^2 - \left(x^2 + y^2 + z^2\right)}{\left(x^2 + y^2 + z^2\right)^{5/2}} \tag{2.13}$$

The magnetic field of a dipole as described by equations (2.11),(2.12),(2.13) can be fitted to measured SSM data. An example of a simulated dipole is displayed in figure 2.5.

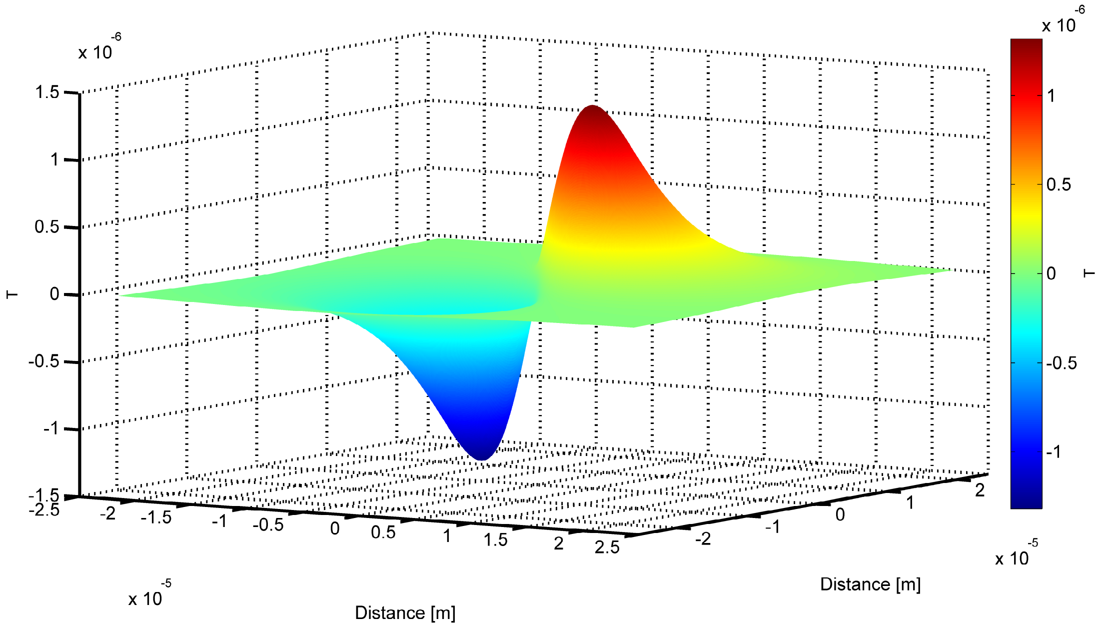

Figure 2.5: A simulated in plane magnetic dipole. Modeled using the equations: (2.11),(2.12),(2.13)

Chapter 3

Experimental setup

3.1 Equipment

Figure 3.1 gives a schematic view of the components of the SSM. A SQUID only operates at low temperatures. Therefore the SQUID and sample are submerged into a large cryostat filled with liquid helium, which is at 4.2 K. The cryostat has an estimated capacity of 70 l and 100 l liquid helium is require to fill it when it is at room temperature. The setup cannot operate if the helium level is below 10%. At this point the temperature of the SQUID sensor is higher than its critical temperature. A cool down of the SQUID sensor and sample into the helium evaporates between $3-5\%$ of helium. This number depends on the speed of the cool down. It is recommended to slowly cool down the sensor and sample. The vacuum of the cryostat can be as low as $2 \cdot 10^{-5}$ mbar. At this pressure a completely filled cryostat contains enough helium to measure for ten days. The measuring time is decreased when multiple cool downs are made. After seven months the vacuum pressure is down to $4 \cdot 10^{-3}$ mbar. This vacuum can only hold helium for five days. It is recommended that the vacuum is pumped down every five to six months to keep the helium loss at a minimum.

A computer is connected to a motion controller. The motion controller can move the sample in the X,Y and Z direction, towards and parallel over the sensor. A homemade program called npscan or an external connected joystick can control the motion controller. Furthermore, the npscan program is also the standard program employed to measure the samples. The controller is connected through GPIB to the computer. The motors are connected through a long rod with the sample holder. The motors operate at room temperature. In the tube going from the motors to the sample holder the rod is connected with a pivot point, see figure 3.2. This point works as a lever and makes that a movement on top is a half a movement at the sample. The software takes this into account. For our SSM setup this ratio is two. This lever causes the sample which is connected to the end of the rod to have a spherical motion. If motion is small, it can assumed that it is flat. However a spherical motion means that there is a height difference between the senor to the sample in one measurement. If the sample is not completely in the center and if there are no strong signals originating from the sample, the spherical motion of the sample can be seen in a measurement.

The SQUIDs flux locked loop is controlled using the Star Cryoelectronics the PCI-100. The PCI-100 is connected to the computer using an USB connection. The PCI-100 box locks a flux into the SQUID. The Star Cryoelectronics measures the SQUID output signal that corresponds to an amount of flux. This signal goes through a low pass filter to reduce high frequency noise and is amplified to emphasis the voltage change.

The National Instruments A/D convertor converts the analog amplified signal to a digital signal. The analog input of the A/D convertor is $\pm 10V$. The A/D convertor is 16 bit and divides the $\pm 10V$ to $\pm 32768(2^{16})$ data points. The npscan software measures these data points.

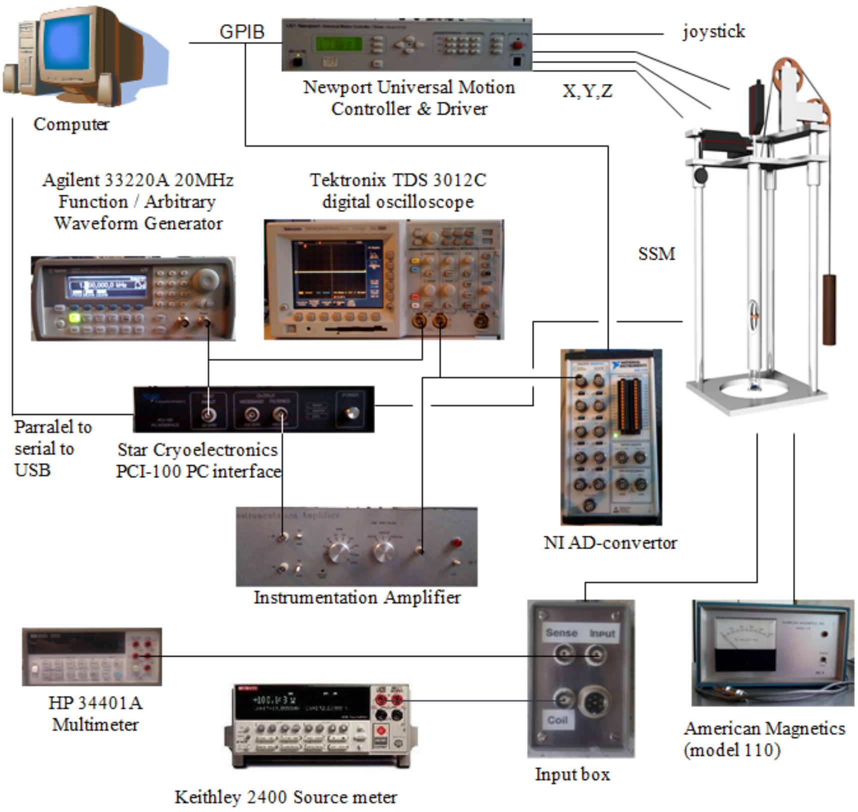

Figure 3.1: A schematic view of the equipment used in the SSM. The black lines show how the equipment and how they are coupled together. This an updated figure version of the ICE SSM user manual.

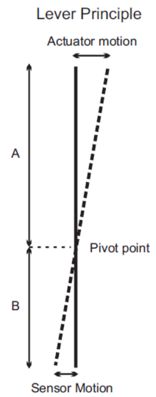

Figure 3.2: The lever mechanism in the SSM. The SSM motors are on top and the sample at the end of the rod. This figure was published in [22].

In the input box there are 12 connections. The first connections go to the coil which is located around the sensor and sample. The coil is used to generate an external magnetic field. The sample and sensor are in the center of the coil. The maximum external field ranges up to a few milliTesla. Too high currents might damage the wiring or connections of the coil. The coil in the SSM has a diameter of 5.6 cm and has 700 windings. Since the sample and sensor are centered inside the coil the Biot-Savart equation is reduced to the magnetic field inside the center of a loop see equation (3.1).

$$B = \frac{\mu_0 I}{2R} \tag{3.1}$$

The magnetic field is directly coupled to the current. For our setup this is roughly $15\mu T$ per milliAmpere. The highest current used is 100 mA.

The top two connections are the strain gauge input/output of the Wheatstone bridge located on the holder. The strain gauge measures whether the sensor is in contact with the sample. This is still done with an analog signal. In the future new software can read this signal digitally using the National Instruments A/D convertor.

The last connector contains the spare wires and the connections that are used for a diode temperature sensor. The temperature sensor is located next to the SQUID and sample in the liquid helium. With the new upgrade the setup can be pumped down. Pumping down the setup decreases the temperate of the liquid helium. The SSM gets a theoretical temperature between 1.5 K and 4.2 K. The temperature dependence can be interesting for studying low temperature superconductors and Topological Superconductors.

3.2 Holder

The SQUID holder contains a lot of parts. Among others it contains the SQUID sensor. The device for measuring the flux. Also the cantilever is vital for a good operation.

It is important for the pickup loop of the sensor to be as close as possible to the sample to measure the strongest magnetic response. A way to achieve this is to place the SQUID sensor on the very end of a cantilever. The pickup loop sticks out in front of the cantilever, as seen in figure 3.3(a). When the sample approaches the holder the tip of the SQUID sensor touches the sample making the cantilever bend. The angle of the cantilever on the holder is 30°.

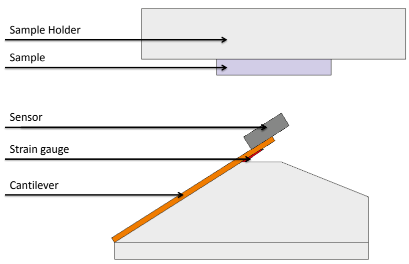

(a)

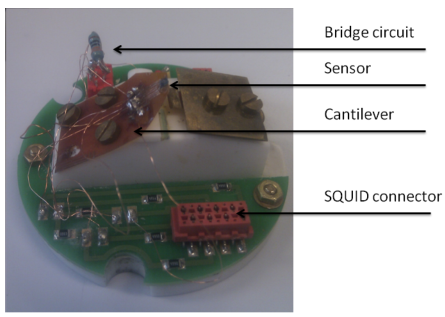

(b)

Figure 3.3: (a) A schematic drawing of the cantilever mounted on the holder. The SQUID sensor is on top and a strain gauge is at the back of the cantilever. (b) An optical image of the holder and cantilever before it is mounted in the SSM.

3.2.1 Sensor

On the top of the holder, the SQUID sensor is glued to the cantilever. The sensor is cut to make sure the pickup loop is at the edge of the sensor. The distance from the pickup loop to the edge of the sensor on a uncut sensor is estimated between 0.5 - 1 mm. This distance varies from sensor to sensor. It depends on where the sensor is located on the wafer and how the wafer is cut. The distance from the pickup loop to the edge of the sensor should be a few micron to get a good resolution.

Cutting a sensor is a time consuming process. In previous years it was done by placing the sensor in a holder and stroking it on sandpaper to scrape off parts of the sensor until the pickup loop was at the edge of the sensor. This process could take up an entire day. To speed up this process a dremel is used. The SQUID sensor is glued into a modified alligator clip using wax. The force at which a alligator clip presses on a sensor is relatively high and it is pressing directly on the SQUID electronics which on the sensor. The beak of the alligator clip is in the shape of a sawtooth. This makes the contact area between the sample and clip very small. To increase the contact area and thus distribute the force over a larger area, the beak of the alligator clip is covered with two component epoxy glue modeled in such a way that the force is evenly distributed over the sensor.

The alligator clip is placed on a holder. The sensor can only move in the X and Y direction. Further sandpaper is placed on the dremel disk and attached using a screw. The standard dremel disk is small roughly 2 cm requiring the sandpaper to be replaced frequently. Therefore a special aluminum disk is created. The disk has a diameter of roughly 6 cm. On the disk sandpaper is glued on using scotch glue, instead of being screwed on. Also the dremel should be clamped on the work bench. The dremel vibrates heavily when cutting. Since the cut must be accurate in the order of a few micron, it is difficult to keep it stable by hand, making a miss cut more likely.

Cutting of the sensor is done under an optical microscope to make the pickup loop visible. The sensor should only be in contact with the sandpaper for short periods of time. The contact with the sandpaper on the dremel heats up the sensor. The sensor can be cooled using water. During the cutting of the sensor dirt accumulates over the sensor. This should be cleaned using water and for example a cotton stick. The first part can be cut relatively fast using rough sandpaper (P1000). When the edge of the sensor is about 20-30 μm from the pickup loop, soft sandpaper (P4000) should be used. It is best to do the last few micron by hand, without the dremel. The dremel cuts fast and cutting off the pickup loop is an easily made mistake. When the cut is done, see figure 3.4(b). The sensor must be cleaned using the sonic bath with acetone and ethanol.

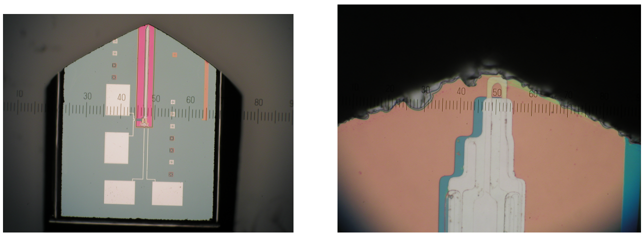

(a) (b)

Figure 3.4: (a) An optical image of a cut sensor were the pickup loop is at the tip of the sensor. (b) A zoomed in optical image of the pickup loop at the edge of the sensor.

3.2.2 Cantilever

The cut SQUID sensor is glued on the cantilever so the tip of the sensor sticks out. The sensor used to be glued with GE varnish mixed with ethanol. Adding ethanol to the glue lowers viscosity of the glue making it easier to place the sensor at the right position. However it also decreases the stickiness of the connection. On occasion it happened that the sensor broke loss from the cantilever while scanning. The breaking might be due to the shrinking of the cantilever at low temperatures and the friction with the sample. If the glue breaks the sensor is still held in place by the wire bonds. A signal can still be locked in SQUID, only the movement is wrong. The only way to detect this is to observe the sensor or touch it gently with for example plastic tweezers. Using GE Varnish without the ethanol solves the problem. When GE Varnish is used it should always be placed inside an over at 100°C for 10 minutes, to harden the glue. A drawing of the cantilever is displayed in figure 3.5.

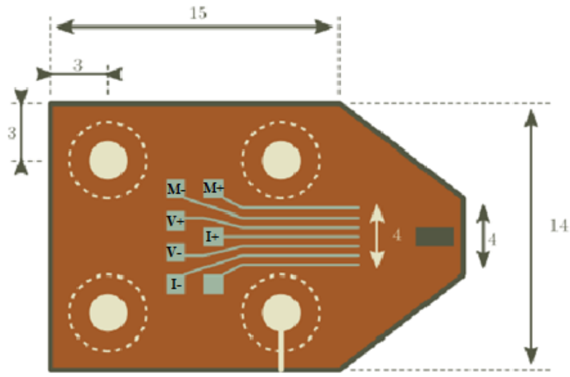

Figure 3.5: A drawing of the cantilever. At one end the SQUID sensor is glued on the cantilever. The coper lines are marked with the name of the connection to the SQUID sensor.

The SQUID sensor is connected by 12 wirebonds to the copper lines on the cantilever. There are four pads on the SQUID sensor. Two for modulation and two for the I-V measurements. Each connection is connected with two aluminum wirebonds. Wirebonds can break during mounting or cooling down the setup. Doubling up on the wires decreases the chance of connection problems during cool down. When a wirebond breaks while the SQUID is in the liquid helium, heating it up and disassembling it for repairs requires much time and helium.

The cantilever is connected to the PC board on the holder using six wires. Thin wires easily break during (un)mounting of the holder, cantilever, sensor or bonding. Wires with a ticker tend to pull out the copper pads from the cantilever. Eventually the thicker wires with a 100 μm diameter were chosen to use on the holder. After soldering on the cantilever the wires are covered with GE varnish to prevent the pads from coming loose.

Wirebonding the sensor pads to the cantilever can give some problems. The sensor contact pads on the sensor are small. It is best to place the bonds at the edge of the pads. If setting a wire fails or if a wirebond breaks it destroys a part of the pad. Therefore a wire in the center of the pas can take the entire pad out if it fails, making it impossible to set any wirebonds on that connection pad. Also do not place wirebonds at the point where the pad is connected to the SQUID loop. Figure 3.6 displays the parts where it is good to set a wirebond (green) and not (red).

The surface of the sensor and cantilever must be clean in order to place a wire. The sensor can be cleaned using the sonic bath and acetone and ethanol. On the cantilever the copper wires are oxidized and covered with glue. This glue must be cleaned with a knife. Acetone and ethanol also dissolve the glue with which the sensor is glued on the cantilever.

The cantilever is flexible and it absorbs the vibration of the wire bonder when a bond is placed. A way around this is to glue the cantilever to the holder or clamping it between the holder and PC board. First set a bond on the cantilever and then on the sensor, making the risk of damaging the sensor as small as possible.

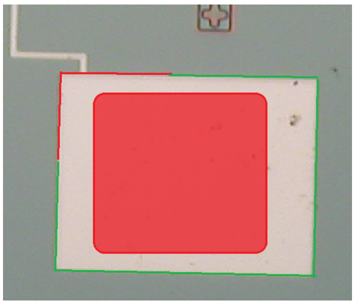

Figure 3.6: A sensor pad of the senor and the locations were to bond given in green and not to bond in red.

Wire bonding damages the copper which is deposited on the cantilever. After replacing four or five SQUID sensors the copper on the cantilever is almost completely depleted. This requires that the complete cantilever should be replaced.

Aligning the sample and sensor has always been a problem. When the setup is submerged into the liquid helium there is no way to see if the sensor is on the sample or not. In the past a telescope was used to estimate the distance between the sample and sensor at room temperature. When the setup is submerged into the liquid helium the assumption is made that this distance is the same. The only way to check if the sensor is at the right position is when a magnetic feature is measured. However if there are no local magnetic features at the spot where the sensor is on the sample, than it is impossible to say if the sensor is on the sample. This makes the risk of crashing the sensor into the sample high. Also measuring at a large distance from the sample without knowing it is one of the possibilities.

This problem is solved by placing a strain gauge at the back of the cantilever. A strain gauge is a resistor which changes resistance on strain. When the sensor is in contact with the sample the cantilever bends and the strain gauge glued on the back of the cantilever changes resistance. It is important to glue the strain gauge directly on the bending point of the cantilever to get optimal response. The resistance is measured using a Wheatstone bridge circuit. Initially the bridge circuit is placed inside the input box. Later the bridge is integrated in the PC board on the holder.

The wires from the cantilever are connected to the electronics on the holder. The electronics on the holder consist out of resistors and connectors. A thin layer of gold is deposited on the holder to conduct the currents. Gold is a very good conductor, however soldering wires and components on thin gold layer can be challenging. The gold dissipates by the heat of the soldering iron and is easily scratched during mounting of the holder. The thin gold layer is replaced by a PC board with copper connections, making the setup more robust and easier to repair. Also the connectors on the holder are changed. The old connectors worked as follows; the male and female components slide past each other making contact. When the setup is cooled down the male and female parts shrink. The male and female connectors shrink at different rates and/or directions making an open connection when submerged in liquid helium. The connectors are replaces by connectors were the male part is clamped in the female part. This way the connection is solid even at low temperatures.

3.2.3 Distance

The distance between the center of the pickup loop and sample can be estimated. The distance between the center of the pickup loop and the edge of the loop is 4.5 μm. The distance between the edge of the loop and the tip of the sensor depends on the quality of the cut of the sensor. The distance between the pickup loop and edge of the sensor is up to one pickup loop diameter. This distance is at the most is 8 μm, usually this distance is smaller. When the sensor is in contact there is an angle between the sensor and the sample. In noncontact mode this angle is 30 degrees. When the sample is in contact the angle decreases to roughly 10 degrees. The lower the angle between the sensor and sample, the closer the pickup is to the sample. However if the angle is too low the wire bonds connecting the cantilever to the sensor touches the sample. The wire bonds touching the sample may damage the sample, wire bonds, or increase the noise in the measurement. The estimation of the distance between the center of the pickup loop and the sample is $sin(10°)·(4.5+8) = 2.1\mu m$.

3.2.4 Photoresist

A sample can be covered with a layer of photoresist. The photoresist is a thin layer of organic material roughly 1 μm thick and uniformly distributed over the sample surface. The tip of the sensor moves through this layer when the sensor is in contact with the sample, see figure 3.7. If the SSM scans a sample the movement of the sensor tip on that sample causes the tip edge to be scratched off, due to the contact mode. This process is slow, but eventually the pickup loop is cut. A soft organic material might help to slow down this process making a sensor last longer. Another advantage is that it is possible to trace the scanned area. When the sensor is cooled down in the liquid helium, it is not possible to see if the sensor is on the sample, now it is possible to check this afterwards. This is especially useful if no magnetic features are measured on the sample, only noise. The alignment of the sensor to the sample changes due to shrinking of the cantilever at low temperatures. The alignment shift is usually only in the Y-direction. In rare cases the sensor can be off sample. Another advantage is that further analysis on the scanned area can be done with other surface analysis techniques like AFM or STM.

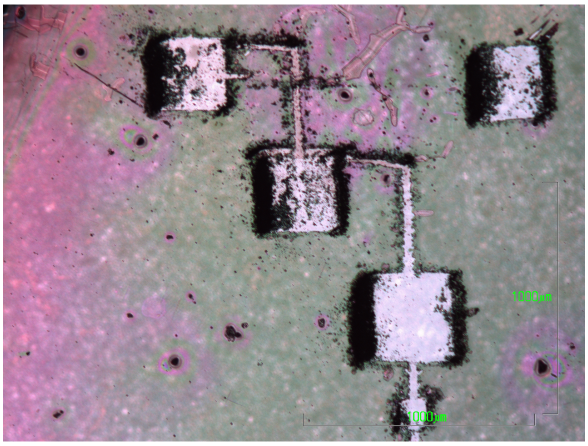

Figure 3.7: Optical image of a TiO_2 sample after scanning. Patches of photoresist are removed by the scanning of the sensor.

3.3 Software

The SSM is operated using two programs. The first is called PCS100. This program is used operate the Star Cryoelectronics PCI-100 box. With this software it is possible to make a flux locked loop. The second program is for approaching the sample and measuring the flux. This program is called npscan. Both programs are needed while scanning.

The PCS100 is an easy to use program. With tune function a modulation for the SQUID can be set if the test signal is on. Figure 3.8 displays what the modulation of the test signal looks like. The signal generator sends out a triangle wave with a frequency of 100 Hz. The output voltage should be set that the asymptote of the test signal are on the same level. As in figure 3.8. This corresponds to one ϕ_0. The peak to peak of the test signal should to be maximized to get an optimal flux to voltage ratio. This is done by changing the bias current so that the signal give out a maximum. After the current is set the modulation and phase can be tuned to maximize the test signal. Then the test signal can be turned off and the SQUID signal can be locked. The locked signal can be centered using the offset. When flux jumps occur the signal can be reset using this program. Typical values for the bias current are 8 μA. If no modulation can be obtained using the setup there is an open connection most likely on the holder. If the test signal has additional or shifted maxima than there is a bad or open connection on the holder most likely being one of the wirebonds.

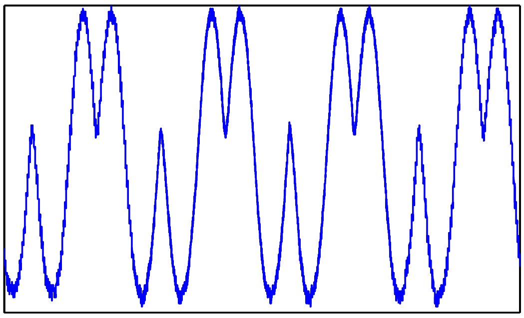

Figure 3.8: A measurement of the test signal of the Star Cryoelectronics PCI-100. This is the proper shape of a optimized test signal.

An open connection can be found measuring the wires coming out of the SQUID. The resistances between M^+ M^-, V^+ V^- and I^+ I^- should be less than one kohm. When measuring something on the SQUID sensor always set the multimeter to measure high resistances at least one Mohm. This is to protect the SQUID from high currents.

The scanning software for the SSM is a homemade program called npscan. This is very old software and it can be a bit tricky to use it. The program crashes a lot. The good thing is that when the program crashes it remembers all the set settings. Also do not alt+tab or move another window over it. It makes values disappear. For example in one incident the Z axis value disappeared and the sample crashed into the sensor.

The npscan saves the data in an unknown format. The format can be read by another homemade program called winimage. With this program the measured data can be displayed. The files can be converted to ASCII characters using the programs bintoasc and dos4gw. The programs only work on a 32 bit computer. Don't use the conversion programs on the original data always a copy. A mistype cannot be corrected and in the worst case the program overwrites the original data.

A start is made on a new SSM program with Labview. At this point the program is not ready for use. It is programmed to scan an area and display the data during scanning. However only the motions are tested on the ESP motion controller. The data acquisition is only tested using a virtual device and saving the data is not integrated into the program.

3.4 Signal

Before any analysis on the measured data can be done, the flux value per data point has to be aquired. To setup this equation it is important to know how the signal is build up. The Star Cryogelectric equipment with the flux locked loop mode gives a $\phi - to - V$ ratio. The voltage is amplified with a gain which can be set from 1 to 100 times. After the amplification the analog signal is converted to a digital signal using an A/D convertor which has 2^{16} points per $\pm$10V.

$$\phi_s = \frac{1}{\phi - to - V \cdot Gain \cdot \frac{2^{16}}{20}} \cdot (N - N_b) \tag{3.2}$$

Equation (3.2) gives us the flux through the SQUID (ϕ_s). Which is now converted from the values of the npscan software (N) mines the background values (N_b). The working point of the FLL is often not exacty at 0 V, this offset can be compensated with N_b [24].

Yttrium barium copper oxide (YBCO) is a well studied high temperature superconducting material. So studying this material can give us a good indication of the quality of our setup. For our measurements two YBCO samples were made. Both samples were thin YBCO films with one being structured varying lines widths. When an external magnetic field is applied when cooling down Abrikosov vortices freeze into the superconductor. Figure 3.9 displays a measurement on a structured YBCO film. In this measurement Abrikosov vortices appear in between the stripes in the YBCO.
The lateral size of a single vortex at the surface of a superconductor is very small. The radius when

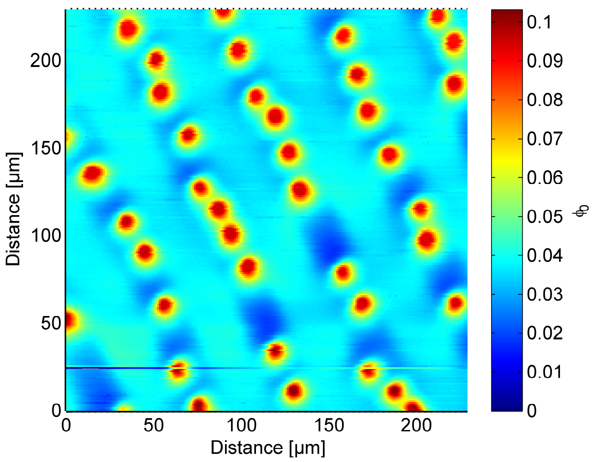

Figure 3.9: Measurement on structured YBCO. Vortices appear in between the lines of the structured YBCO.

the field of a vortex decays is comparable with the landau penetration depth λ_L, which is in the order of 200 - 300 nm for YBCO at T = 4 K [25]. The vortex core is much smaller than the distance of the pickup loop to the vortex, which is in the order of a few micrometer . The assumption is made that $d >> \lambda_L$ where d is the distance to the pickup loop. That makes the equation for the magnetic field of a vortex as equation (3.3) [26].

$$B(\vec{r}) = \frac{\phi_0}{2\pi r^3}\vec{r} \tag{3.3}$$

When the pickup loop is centered directly above the vortex, the most flux flows through the pickup loop. In the measurement setup the pickup loop with radius (r), is at a certain height (h) above the vortex. With this in mind it is possible to calculate the magnetic field through the pickup loop, giving us equation (3.4).

$$\phi_{loop} = \phi_0 \left(1 - \frac{h/r}{\sqrt{(h/r)^2 + 1}}\right) \tag{3.4}$$

The signal of a vortex decreases exponentially with distance. As can be seen in figure 3.10. Measured vortices in YBCO have the highest value at $0.1\phi_0$. This corresponds with a distance of 3.1 μm above the sample. A nicely cut sensor is crucial for having a good resolution.

The step size of the measurements is much smaller than the diameter of the pickup loop. The pickup loop has a inner diameter of 3 μm and the step sizes are usually between 0.4 and 2 μm. Therefore the flux that goes through the pickup loop is larger the flux coming from the pixel area (A_p) its centered above. The flux through the SQUID is a convolution of the magnetic field with

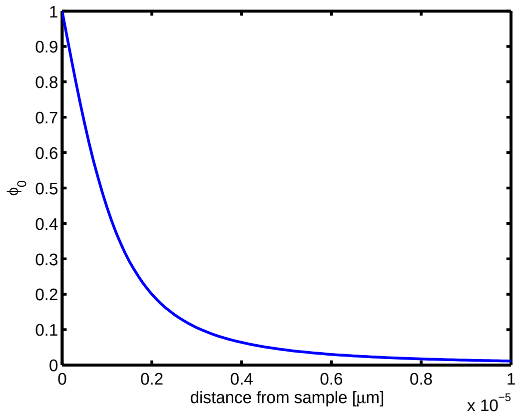

Figure 3.10: The picked up flux by the pickup loop from a vortex versus the distance from the sample.

the effective area (A_s) of the SQUID sensor. If a measurement requires integration of the magnetic field, of for example a vortex, it is import to keep this effect in mind. The area of the pickup loop is not the effective area of the SQUID. Due to flux focusing and the coupling factor the effective area changes. Also the leads to the pickup loop and SQUID itself can have an effect in the measured flux. The assumption is made that the flux going through the pickup loop is uniformly distributed, than the flux through a pixel (ϕ_p) is defined as equation (3.5).

$$\phi_p = \phi_s \frac{A_p}{A_s} \tag{3.5}$$

The flux through an area is the same as the sum of all the individual flux through the pixels in that area. Combining equation (3.2) and (3.5) results in equation (3.6).

$$\sum \phi_p = \frac{1}{\phi - to - V \cdot Gain \cdot \frac{2^{16}}{20}} \frac{A_p}{A_s} \cdot \sum (N - N_b) \tag{3.6}$$

Figure 3.11(a) displays a single isolated vortex. The flux of one vortex is quantized and equal to one ϕ_0. The sum of the measured flux over the area of a the vortex is equal to one ϕ_0. By summing up the flux in the vortex, the ratio $\frac{A_p}{A_s}$ from equation(3.6) is determined. The effective area of this sensor is 5.4 μm^2.

3.5 Noise

The SSM is very sensitive to external noise sources, for example mobile phones or electronic devices connected to the mains can interfere with the measurements. A spectrum analysor is used to measure the noise level. It reads the output of the SQUID cooled down in the liquid helium and with a flux locked loop. All excessive wiring in the SSM setup is removed and the remaining wires are as short as possible. Also all electrical equipment in the vicinity is disabled. The measured data is the averaged over five measurements. The measurements were done with the same SQUID sensor. The noise level decreases drastically at one kHz for both measurements, this is because of the low pass filter that is in the electronic circuit, to reduce high frequency noise. Figure 3.12 displays a noise spectrum of the SQUID sensor during the day (the red line) and at night (the blue line).

The measurement at night gives us white noise with a base noise level which is about 14 $\mu\phi_0/\sqrt{Hz}$. Turning on electrical equipment which is connected to the mains and in the vicinity of the SSM created a clearly visible spike at 50 Hz. For example the strain gauge multimeter creates a spike at 50

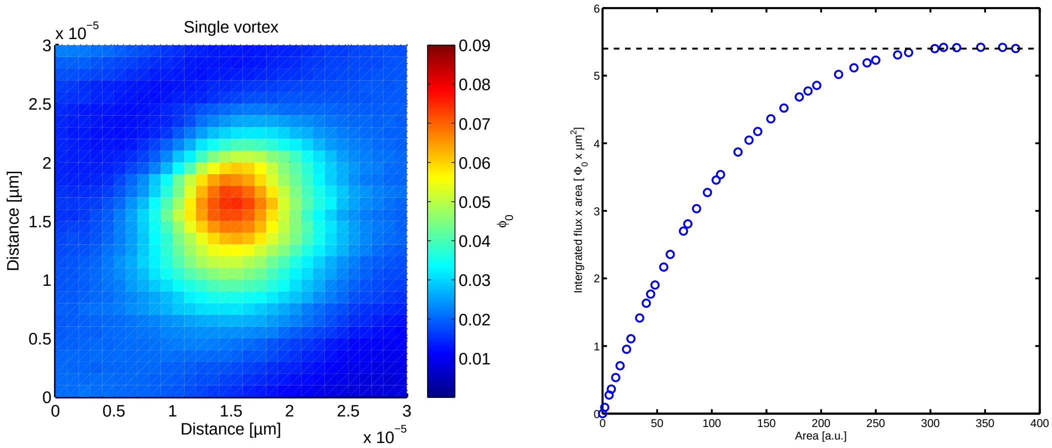

(a) (b)

Figure 3.11: (a) A single isolated vortex in a YBCO film. The vortex has a maxima around 0.09 ϕ_0. (b) The summation of the flux of the isolated vortex.

Hz which is at least two times higher than the base noise level.

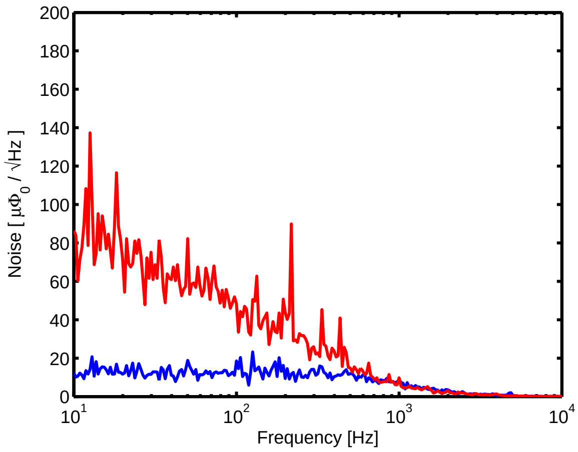

Figure 3.12: The noise spectrum of a day (red) and night(blue) time measurement.

There are some difference between the day and night time measurements. In daytime measurements not all equipment in the vicinity of the SSM is disabled. Other experiments were either being prepared or executed in the same room as the SSM setup and the lab directly next to the SSM setup. Also during the daytime measurement sensor was cooled down with field cooling. The noise during the daytime is pink noise and much higher than during the night. These measurements represent the best and worst case in terms of noise levels. High sensitive measurements should be done at night to get an optimal resolution.

Another common noise source which should be highlighted are mobile phones. When a phone makes contact with a communication tower it sends of a signal which is also picked up by the SSM. This signal is so strong that overwhelms the SQUID making it impossible to observe any signals from the sample. Therefore it is also good to test the influence of these noise sources. Only mobile phones that are in the room with the SSM cause interference. Phones that are outside the room either in the hallway, outside or on the floor above the SSM did not show an observable interference.

Chapter 4

Results

4.1 Ferromagnetism at the $LaAlO_3/SrTiO_3$ interface

4.1.1 Introduction

In September 2011 a paper was published about the coexistence of ferromagnetism and superconductivity at a $LaAlO_3/SrTiO_3$ (LAO/STO) interface. The coexistence of ferromagnetism and superconductivity is rare, because superconductivity breaks down with magnetism. The combination of the two materials LAO and STO is very interesting match. LAO and STO are both nonmagnetic insulating materials, but when together as thin films the interface between them becomes conducting. At certain growth conditions it can even be superconducting at low temperatures (300 mK). The Moler group at Stanford University uses scanning SQUID imaging on the LAO/STO interface. Using their SSM a landscape of ferromagnetism, paramagnetism and superconductivity is found. There are several possible reasons for the magnetism appear. The first is found with the help of Density functional theory(DFT). When theory is applied to a perfect interface it finds a number of nearly degenerate states. Some of these states have a spin polarization and thus gives rise to magnetism. A second possibility is the existence of oxygen vacancies at the LAO/STO interface. The oxygen vacancies make a polarized unit cell which can give rize to magnetism.[27, 28]

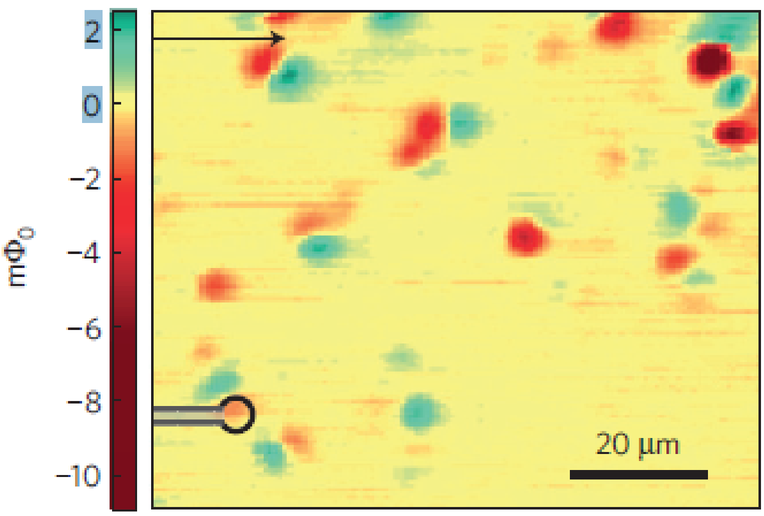

Figure 4.1: A SSM measurement from Stanford university on the LAO/STO interface showing a landscape of dipoles. This figure was published in [27].

Sample number	LAO thickness	Growth pressure	Remarks
1	20 UC	$2 \cdot 10^{-3}$ mbar	Old sample
2	26 UC	$2 \cdot 10^{-3}$ mbar	Old sample
3	20 UC	$1.3 \cdot 10^{-3}$ mbar	Singapore sample
4	10 UC	$2 \cdot 10^{-5}$ mbar	Sample made with the Stanford settings

Table 4.1: The different LAO/STO samples that are measured by the SSM.

The ferromagnetism forms as spatially separated dipoles as seen in figure 4.1. The dipoles remain stable for the entire measurement time of one month and are not temperature dependent. The dipoles found in the samples in Stanford have a strongly varying density and a magnetic moment of typically $10^7 \mu_B$ but up to $10^8 \mu_B$. The dipoles have a random orientation and no net magnetization. Also gating did not have a observable effect on the ferromagnetism. The thickness of the samples range from 0 to 16 LAO layers. There was magnetism observed below the critical thickness of 3 UC LAO.

The LAO layers were grown on TiO_2 terminated (001) STO substrates. The LAO is deposited at a pressure of $1.3 \cdot 10^{-5}$ mbar at $800°C$ and a oxygen pre anneal at a pressure of $5 \cdot 10^{-6}$ mbar and $950°C$ for 30 min. After the deposition the samples were cooled down to $600°C$ and annealing in a high pressure at 0.4 bar in an oxygen environment. The films were locally scanned on the composition to rule out the possibility of contamination. The samples show very weak magnetic features such as dipoles or a magnetic landscape. But not higher then also seen on non magnetic samples.

The magnetometry was done with a scanning squid microscope with a pickup loop of three micron. The pickup loop is about 1 micron above the sample. The scanning SQUID microscope used during these measurements has a sensitivity of 0.7 $\mu\phi_0/\sqrt{Hz}$. The background noise level is lower than our setup. However our SSM should still be able to detect these magnetic features.

4.1.2 Results

To verify these experimental results we tried to confirm the ferromagnetism in our LAO/STO samples. In total four different samples were tested. Two of the samples are already existing samples, already used in other types of experiments. One sample was made in Singapore and one sample was made to the exact specifications as the experiments in Stanford.

Note that sample number four is grown on the same conditions as the samples in Stanford. Low growth pressures causes the particles in the plasma to reach the target at higher speed and thus energy, making it more likely to create oxygen vacancies. No dipoles or magnetic features were measured above the noise level on the sample 1,3,4. Figure 4.2 shows a typical measurement on these samples. This measurement was done on sample three.

The scanned area was on each sample is between 0.64 mm^2 and 1 mm^2. Only on the second sample a total of four dipoles were measured. The total scanned area on this sample is 1 mm^2. All the dipoles are located at one location. The maximum distance between the dipoles is not more than 200 μm. The magnetization of the dipoles is calculated using the dipole model described in the theory. Since the dipoles are assumed to be an interface effect in the LAO/STO interface, the assumption is made that this is in-plane magnetization. So there is no magnetization in the Z direction (Bz=0). Fitting the model to the dipoles gives us the magnetization of the magnetic moment around $5 \cdot 10^{-8} \mu_B$. A fit is shown in figure 4.3. The spatial width of the dipoles ranges up to 25 μm. Measurements were done using field and zero field cooling, but no difference was observed.

The 26 UC LAO/STO sample was created over a year ago and has suffered a lot of testing. This makes the chance that the sample has been contaminated high. Together with the very large magnetization and the very low density of the dipoles this makes it unlikely that the signal originated from the interface of the sample. In conclusion in our samples no ferromagnetism in the LAO/STO

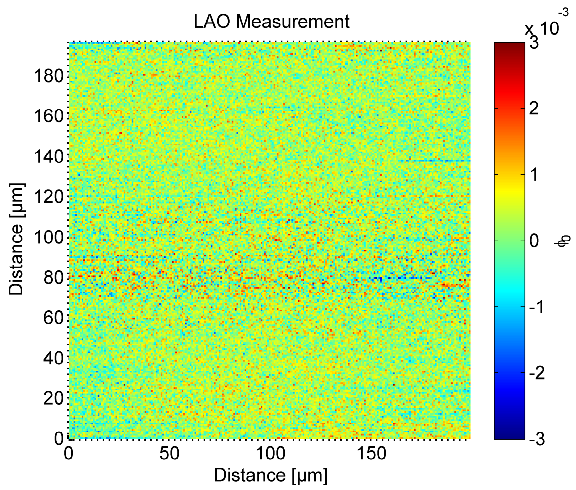

Figure 4.2: A typical LAO/STO SSM measurement. No magnetic features appear above the noise level.

interface as described by the papers from the Moler group in Stanford was observed. Even sample grown with the same specifications did not deliver the same results.

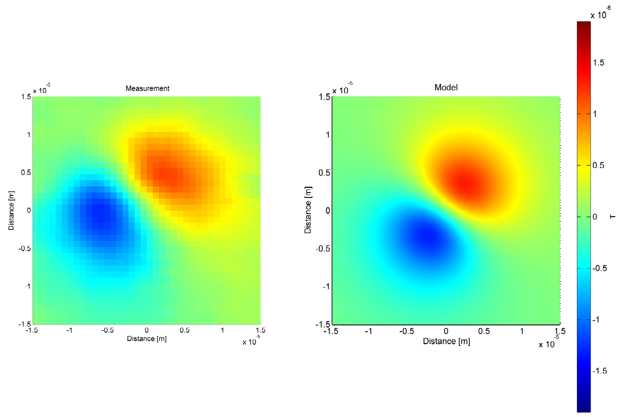

Figure 4.3: On the left a measured dipole and on the right the fit of the measured dipole.

4.2 Ferromagnetism in $\mathrm{Ti_{(x\text{-}1)}Ta_xO_2}(\mathrm{x} \approx 0.05)$

4.2.1 Introduction

In collaboration with the National University of Singapore the magnetic features of doped Titanium dioxide (TiO_2) were tested. The TiO_2 is grown on $LaAlO_3$ substrate using pulsed laser deposition (PLD). The TiO_2 samples are doped with Thallium. Using normal SQUID measurements the magnetization peaked at a doping level around $5-6\%$. The measured field of the $Ti_{(x-1)}Ta_xO_2$ $(x \approx 0.05)$ is around 70-90 Oe. Analysis revealed that the Ta is not directly the cause of the ferromagnetism. The Ti vacancies that are caused by the Ta doping cause the unit cell to have a magnetic moment. When electrons flow passed this vacancy they receive this magnetic orientation. If now the orientated electrons pass though another Ti vacancy they try to flip the moment to the same orientation as the electrons have them self. This theory is called RKKY and this effect in usually found in semiconductors. This also means that the majority of the Ti vacancies are at the interface of the sample [29].

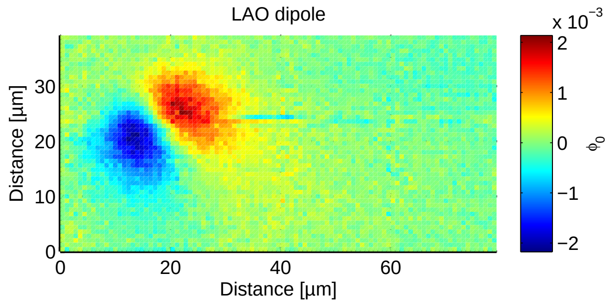

Figure 4.4: A measured dipole on the 26 UC LAO/STO sample. One of only four found dipoles.

4.2.2 Results

Since the $Ti_{(x-1)}Ta_xO_2$ ($x \approx 0.05$) has ferromagnetic magnetization, the surface is expected to have a ferromagnetic features. A SSM is an excellent piece of equipment to verify if this assumption is valid. In total four samples of the Ta doped TiO_2 were measured using the SSM. The samples that were measured have different film thicknesses. The thickness of the TiO_2 films are 10 nm, 37 nm, 350 nm and 400 nm.

Initially the research started with only the 10 nm and 37 nm samples. Figure 4.5 and 4.6 displays the results of a measurement done on these samples.

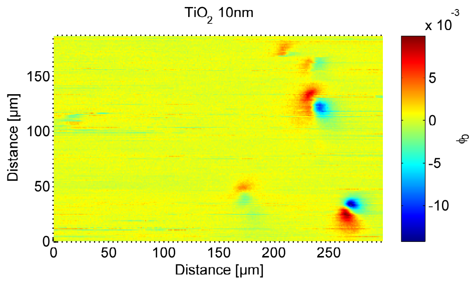

Figure 4.5: A SSM measurement on a Ta doped TiO_2 10 nm film. The measurement show a landscape of dipoles.

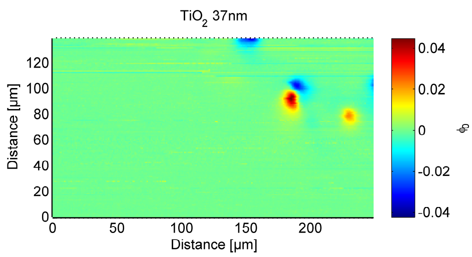

Figure 4.6: A SSM measurement on a Ta doped TiO_2 37 nm film. The measurement show a landscape of dipoles.

Both measurements displayed in figure 4.5 and 4.6 were measured under zero field cooling and both samples have a thin layer of photoresist on them. The measurements show a landscape of magnetic dipoles. On both samples no magnetic domains were observed. The magnetic dipoles appear to have a random orientation. In the 10 nm and 37 nm films dipoles have a spatial density of 1 dipole per 300 x 300 μm^2.

The width of a dipole can be as large as 10 μm. The total scanned area is 0.25 mm^2 on the 10 nm film and on the 37 nm the scanned area is 0.64 mm^2. Both samples visually appear to have dirt on them. As can be seen in figure 4.7(a). After measuring both samples were cleaned. All the photoresist got removed. However after cleaning the dirt on the sample remained. After cleaning the samples were remeasured without photoresist. In these measurements the dipoles remained unchanged in size density and orientation.

Since the magnetic effects may occur at the interface structuring, the sample may have some effect on the dipole orientation and location. After a surface roughness scan with an AFM, the 10 nm thin film has a surface roughness of 8 nm. The 37 nm thin film has a surface roughness of 70 nm. In these films the surface roughness is equal or larger than the film thickness. A possible reason for this is that the photoresist freezes at a temperature of 4 K and while freezing it might have cracked the surface of the TiO_2 films.

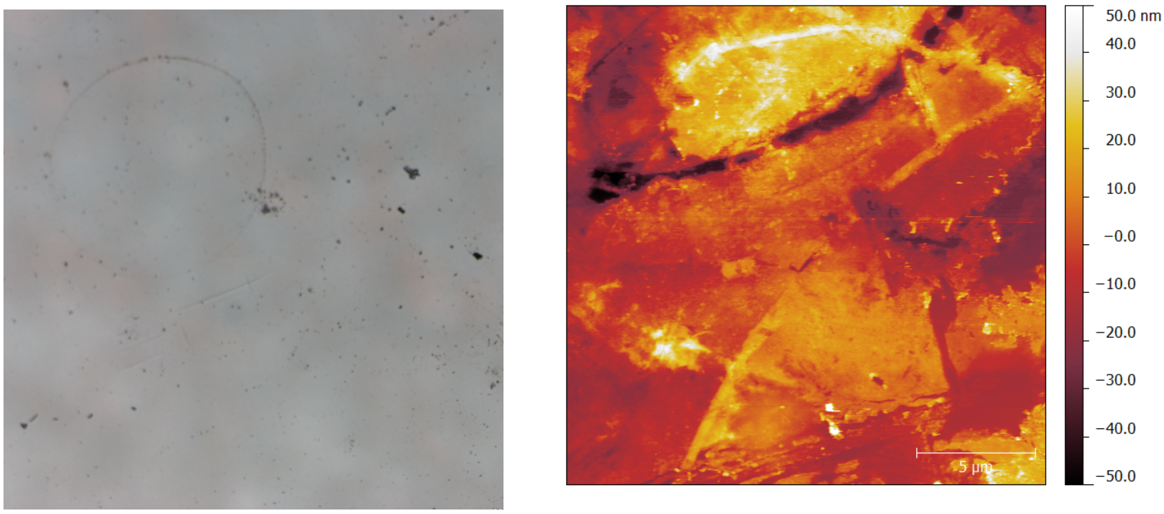

(a) (b)

Figure 4.7: (a) An optical image taken under a microscope displaying the sample surface of the TiO_2 37 nm thin film. (b) An AFM measurement of the surface of of the TiO_2 37 nm thin film. The AFM scanned an area of 20x20 μm.

The two thicker samples were measured with zero field cooling. However no photoresist was applied to these samples to exclude the photoresist from influencing the measurements.

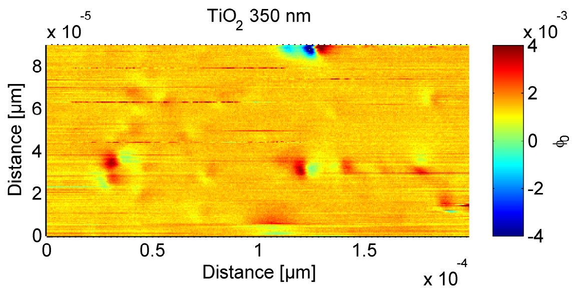

Figure 4.8: A SSM measurement on a Ta doped TiO_2 350 nm film. The measurements show a landscape of dipoles. The dipole density is higher than the thinner films (10 nm and 37 nm).

Figure 4.8 displays a measurement on the 350 nm sample. The 350 nm sample has a much higher dipole density then in the thinner films. The dipole density is here is one dipole per 50 x 50 μm^2. The spatial size and magnetic strength are similar to the 10 and 37 nm films sample. On the last sample the 400 nm thin film no magnetic features were observed. However only one measurement was conducted. The scanned area is 0.2 mm^2.

With applying an external magnetic field one should be able to flip the magnetization of a dipole. However this did not happen. The maximum external field that was applied was 1 mT. Being that this external field has a weak magnetic strength it is very likely that this field too weak to make any change. Also field cooling did not change the strength, density or orientation of the dipoles. No superconducting features such as vortices were observed.

4.3 Imaging of the ferromagnetic insulator $LaMnO_3$

4.3.1 Introduction

The combination of a material being a ferromagnetic and an insulator is rare. A few ferromagnetic insulators have been discovered such as EuO and $YTiO_3$. The working mechanisms of these materials are still under investigation. There might already be applications for these materials. Ferromagnetic insulators are good candidates for spin polarizers or for hard disk applications. In bulk $LaMnO_3$ (LMO) is a Mott insulator, however when grown in thin film the material shows different properties. Thin films of LMO film show to have ferromagnetic properties. The precise origin of the ferromagnetism in these films is still not known. There are two possible origins for ferromagnetism in these films. The first possibility is oxygen vacancies in the material and the second one is due to strain in the film. All the films were made using pulsed laser deposition of LMO on a STO(001) or 0.1% Nb doped STO (001) (NSTO) substrate.

4.3.2 Results

Two LMO samples were made using PLD, a 12 UC and a 24 UC sample. The LMO films have a resistance of more than one MOhm in the temperature range from 2 K to 300 K, making it an insulator. Next to general conduction across the sample also the local conduction was tested using a conducting AFM. The samples were also locally insulating. Using the SSM the surface of the sample was scanned on local magnetic properties at a temperature of 4 K. Figure 4.9 displays SSM measurements on the 12 UC and 24 UC films.

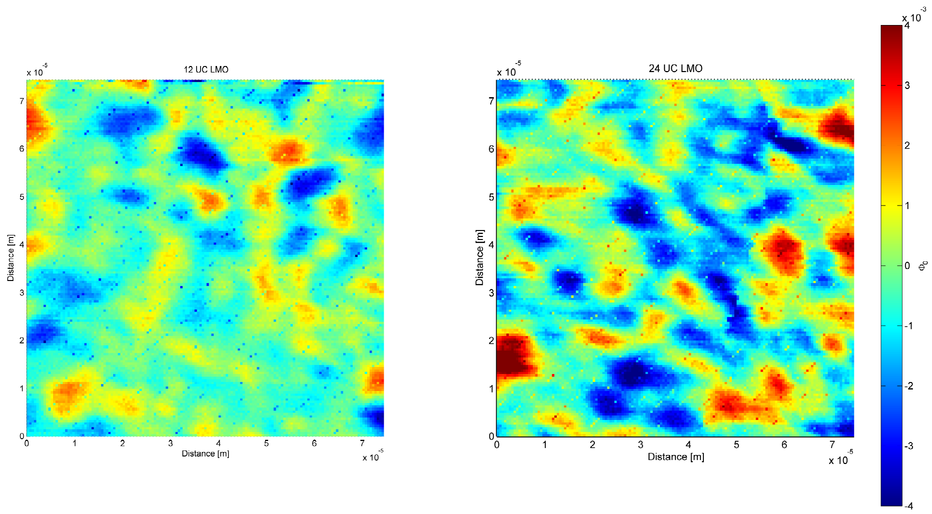

Figure 4.9: SSM measurements on different LMO samples. A 12 UC sample (left) and a 24 UC sample (right). Both measurments show ferromagnetic domains. The flux strength on the 24 UC is larger than the 12 UC sample.

The measurements show a magnetic landscape. All measurements on the LMO films show this type of landscape. The red color represents out going flux and the blue color the in going magnetic flux. The maxima of the magnetic flux are $\pm 4m\phi_0$. Comparing the 12 UC and 24 UC samples its shown that the spatial size of the domains is the same. The thicker 24 UC sample shows a higher number of counts of higher flux values. The magnetic flux going in and out of the sample is higher in the 24 UC sample then in the 12 UC sample. This corresponds with the normal SQUID measurements. From this data we can conclude that de LMO is a ferromagnetic insulator.

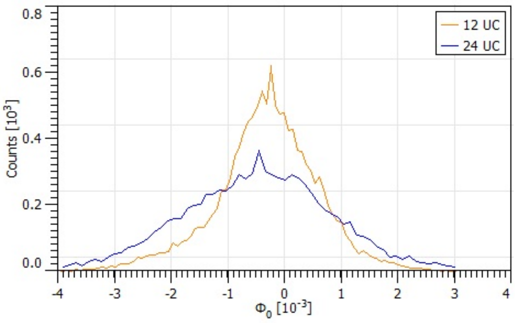

Figure 4.10: The graph displays the number of pixels with a certain flux value. This data is taken from the measurents in figure 4.9. Both measurements have the same amount of pixels. The 24 UC has a higher number of high flux pxels.

Chapter 5

Conclusions and recommendations

The SSM is a complex device, mastering it takes much time. In return the machine can map the magnetic flux over surface accurately. After 1.5 years of being out of service it required about 1.5 months to obtain a first measurement. At the start of the project the SSM could only operate for maximally one week before it required repairs. Finding the problems and repairing them required one to two weeks. In the first months there were only a few weeks of measurement time. The modifications at the holder (especially the PC board), cantilever, sensor and gaining experience on the operating the SSM increased the durability. At the end of the project it is possible to keep the SSM continuously operational for two months. The improved fabrication techniques and the more robust SSM decreased the repair time. The replacing the sensor typically requires two - three days.

Changes have been made to the SSM setup. However the setup can still be improved. A lot of changes that were made were regarding making the setup more user friendly and robust. Some changes are already being constructed but not jet implemented into the system. The first is that a niobium shield is placed around the sensor and sample. Blocking external magnetic interference. A second is the option to cool down to lower temperature by lowering the pressure in the system. This option includes a temperature sensor. Also a large helium exhaust has been placed to reduce the filling time of the helium. The exhaust was small making the time to fill the SSM with helium between a half and one day.

The software should be replaced by new software in for example Labview. The current software npscan crashes a lot. This can cause the sensor to crash into the sample. Also the conversion program that converts the npscan data to ASCII characters only works on a 32 bit system.
The distance of the pickup loop to the sample surface should be as close as possible. The angle between the sensor and sample is one of the parameters that determine this distance. In the SSM setup this angle can be made smaller without damaging the wirebonds during measurements. This can be changed by placing the cantilever at a smaller angle at the holder.
In 2008 a paper was published [30] were they used mathematical techniques to improve the spatial resolution of a SSM. It might be interesting to see if this or similair techniques can be used on the SSM in Twente.
The ability to do susceptibility measurement with the SSM would be interesting. This requires a different type of sensor. The SQUID sensor has to have an integrated field coil for these types of measurements. In the past these sensors were used on the SSM in Twente. There is no reason why this cannot be integrated in this setup.
One of the sample holders can be modified so a sample can be bonded to it, so gating experiments can be preformed.

Some materials were measured using the SSM. The Moler group at the Stanford University found ferromagnetism and superconductivity at a LAO/STO interface. The ferromagnetism appeared in the form of dipoles scattered over the sample. Different homemade LAO/STO samples were tested on the same ferromagnetism. Of the four samples only one sample (the old 26 UC sample) contained dipoles. The total amount of four dipoles were measured. The dipole are concentrated at one location. Even the samples made with the same parameters as in Stanford did not produce the same results. The claim that our samples have ferromagnetism is not one that can be made using this data.

On the TiO_2 sample a landscape of dipoles were found on the different samples. The measured dipoles have a random orientation. The dipole density increased with the thickness of the film. No domains and vortices were observed in these films. The last material that was investigated is LMO. On LMO ferromagnetic domains were found across the whole sample. The flux on the surface of a sample increases with film thickness. LMO is an insulating material. This makes LMO a ferromagnetic insulator.

Bibliography

[1] Binnig, G., Quate, C. F., and Gerber, C. (1986) *Physical Review Letters* **56**, 930.

[2] Binnig, G., Rohrer, H., Gerber, C., and Weibel, E. (1982) *Physical Review Letters* **49(1)**, 59.

[3] Jaklevic, R. C., Lambe, J., Silver, A. H., and Mercereau, J. E. (1964) *Advances in Physics* **12(7)**, 159.

[4] Vu, L. N. and Harlingen, D. J. V. (1993) *IEEE Transactions on Applied Superconductivity* **3(1)**, 1918.

[5] Davidy, B., Grundlerz, D., Kreyz, S., Doormanny, V., Eckarty, R., Krummey, J. P., Rabey, G., and Doessely, O. (1996) *Superconductor Science and Technology* **9**, 4A.

[6] Kirtley, J. R., Tsuei, C. C., Moler, K. A., Kogan, V. G., Clem, J. R., and Turberfield, A. J. (1999) *Applied Physics Letters* **74(26)**, 4011.

[7] Kirtley, J. R., Ketchen, M. B., Tsuei, C. C., Sun, J. Z., Gallagher, W. J., Yu-Jahnes, L. S., Gupta, A., Stawiasz, K. G., and Wind, S. J. (1999) *Advances in Physics* **48(4)**, 449.

[8] Sandhu, A., Kurosawa, K., Dede, M., and Oral, A. (2004) *Japanese Journal of Applied Physics* **43**, 777.

[9] Kirtley, J. (2002) *Physica C* **368**, 55.

[10] Huber, M. E., Koshnick, N. C., Bluhm, H., Archuleta, L. J., Azua, T., Bjornsson, P. G., Gardner, B. W., Halloran, S. T., Lucero, E. A., and Moler, K. A. (2008) *Review of Scientific Instruments* **79(5)**, 053704.

[11] Kirtley, J. and Wikswo, J. P. (1999) *Annual Review of Materials Research* **29**, 117.

[12] Wu, M. K., Ashburn, J. R., Torng, C. J., Hor, P. H., Meng, R. L., Gao, L., Huang, Z. J., Wang, Y. Q., and Chu, C. W. (1987) *Physical Review Letters* **58(9)**, 908.

[13] Bardeen, J., Cooper, L. N., and Schrieffer, J. R. (1957) *Physical Review* **108**, 1175.

[14] Yun, S. H. and Wua, J. Z. (1996) *Applied Physics Letters* **68(6)**, 862.

[15] Josephson, B. D. (1962) *Physics Letters* **1(7)**, 251.

[16] Jansman, A. B. M. High-Tc dc SQUIDs for use in a background field PhD thesis University of Twente (1999).

[17] Cyrot, M. and Pavuna, D. (1992) Introduction to superconductivity and high-Tc materials, World Scientific Pub Co Inc, .

[18] Stewart, W. (1968) *Applied Physics Letters* **12**, 277.

[19] McCumber, D. (1968) *Journal of Applied Physics* **39**, 3113.

[20] Clakre, J. and Braginski, A. (2004) The SQUID Handbook: Vol.1 Fundamentals and Technology of SQUIDs and SQUID Systems, Wiley-VCH, first edition.

[21] Koch, R. H., Rozen, J. R., Woltgens, P., Picunko, T., Goss, W. J., Gambrel, D., Lathrop, D., Wiegert, R., and Overway, D. (1996) *Review of Scientific Instruments* **67(8)**, 2968.

[22] Troeman, A. G. P. NanoSQUID Magnetometers and High Resolution Scanning SQUID Microscopy PhD thesis University of Twente (2007).

[23] Adamo, M. Nappi, C. and Sarnelli, E. (2008) *Measurement Science and Technology* **19(1)**, 015508.

[24] Verwijs, C. J. M. Fractional flux quanta in high-Tc/low-Tc superconducting structures PhD thesis University of Twente (2009).

[25] Lee, J. and Lemberger, T. R. (1993) *Physical Review Letters* **62(19)**, 2419.

[26] Kirtley, J. R., Ketchen, M., Stawiasz, K. G., Sun, J. Z., Gallagher, W. J., Blanton, S. H., and Wind, S. J. (1995) *Applied Physics Letters* **66(9)**, 1138.

[27] Bert, J. A., Kalisky, B., Bell, C., Kim, M., Hikita, Y., Hwang, H. Y., and Moler, K. A. (2011) *Nature Physics* **7(10)**, 767.

[28] Kalisky, B., Bert, J. A., Klopfer, B. B., Bell, C., Sato, H. K., Hosoda, M., Hikita, Y., Hwang, H. Y., and Moler, K. A. (2012) *Nature Communications* **3(922)**, 1931.

[29] Rusydi, A., Dhar, S., Barman, A. R., Ariando, Qi, D., Motapothula, M., Yi, J. B., Santoso, I., Feng, Y. P., Yang, K., Dai, Y., Yakolev, N. L., Ding, J., Wee, A. T. S., Neuber, G., Breese, M. B. H., Ruebhausen, M., Hilgenkamp, H., and Venkatesan, T. (2012) *Philosophical Transactions of the Royal Society A* **370(1977)**, 4927.

[30] Hayashi, M., Kaiwa, T., Ebisawa, H., Matsushima, Y., Shimizu, M., Satoh, K., Yotsuya, T., and Ishida, T. (2008) *Physica C* **468**, 801.

Chapter 6

Acknowledgments

In the final page of my report i would like to thank everyone who I worked with these past ten months. I really enjoyed my time at ICE working on this project. I want to thank Hans for his enthusiasm and suggestions. I also want to thank Michiel Duits for taking part in my Graduation commission. And Jaap for solving some last minute problems.

I would like to thank Peter for his help with this project and the help with my report, Frank and Dick for their help on SSM. Wang Xio It was really fun working with you. And thanks for the games of pool i lost. Alexander Andreski I want to thank you for the help getting the SSM operational. Jeroen, Kai and Werner thanks for the nice lunches and the fun times we had this last year.